Trajectory PHD Filter for Extended Traffic Target Tracking with Interaction and Constraint

Xi Cao, Yunlian Tian, Jiaye Yang, Wujun Li, and Wei Yi
School of Information and Communication Engineering
University of Electronic Science and Technology of China, Chengdu, China
Email: {caoxi0419, yunlian_tian, yangjy991105}@163.com, {1224liwujun, kussoyi}@gmail.com

***Abstract*—With the increasing demand for traffic situation awareness, extended traffic target (ETT) tracking is a significant yet challenging task especially in tough scenarios with dense and various ETTs. Due to the spatial proximity of ETTs and a noisy sensor, it is challenging for multi-target tracking algorithms to effectively distinguish and track ETTs. To improve the accuracy and robustness of ETT tracking in tough traffic scenarios, we analyze the interaction among ETTs and the lane constraint. Firstly, we develop an interactive motion model for collision avoidance to address trajectory confusion when ETTs are in close proximity. Additionally, we propose a lane constraint method that models lanes as pseudo measurements and constrains the motion of ETTs via pseudo update. Considering the complexity and extendibility, the extended target trajectory probability hypothesis density (ET-TPHD) filter is adopted to achieve a more accurate estimation of ETT trajectories. Specifically, we realize the proposed interactive motion model and lane constraint method based on the ET-TPHD (IC-ET-TPHD) filter. Performance comparisons between our proposed filter and other algorithms are conducted through both simulations and experiments.**

***Index Terms*—Extended traffic target tracking, interactive motion, lane constraint, trajectory PHD filter**

I. Introduction

Situation awareness of traffic scenarios, particularly focusing on extended traffic target (ETT) tracking, is crucial for aiding urban traffic management [1] and intelligent transportation systems (ITS) [2]. A range of advanced sensors typically installed on stationary platforms offer real-time and accurate traffic information through the detection and tracking of ETTs, including cars, trucks, buses, bicycles and pedestrians. Firstly, tracking results can reflect traffic flow, aiding in monitoring traffic congestion [3]. Secondly, ETT tracking can detect abnormal traffic behavior, such as sudden deceleration, illegal lane change, etc., prompting swift responses from drivers and traffic management departments to prevent accidents [4]. Moreover, advanced ETT tracking algorithms also enhance path planning and traffic signal optimization. Consequently, developing a novel algorithm improves real-time accuracy is paramount for ETT tracking.

The characteristics among ETTs are close proximity, high density and various sizes, making it difficult to determine which ETT produced the measurement and the association is complex. This complexity confuses the trajectories of neighboring ETTs for tracking algorithms. Moreover, when an ETT is far from the sensor, the large measurement noise degrades the quality of its trajectory obtained by the tracker. However, unlike aerial targets, it is inspirational that ground ETT usually interacts with each other and is constrained by lanes which can be utilized to optimize system models and recursion [5], [6].

When discussing interactive motion, various models are considered. The social force model (SFM), which illustrates pedestrian motion dependence, is examined in [7], [8]. Additionally, some car-following models (CFM) of microscopic traffic flow [9]–[11] describe vehicle dependence. Concepts like boid flocking [12], virtual leader–follower (VLF) [13], targeting group behaviors, are also informative. The road map is utilized as prior information to constrain vehicles [5], [14]. [15], [16] used the road constraint to improve the performance of data association. Furthermore, modeling the target state in the road coordinate system, capturing longitudinal and lateral motion behaviors, proves convenient [17]–[19]. However, to our knowledge, most literature does not simultaneously consider the interaction and constraint in challenging scenarios with dense and various ETTs.

With the enhancement of detection and recognition capabilities in modern sensors, the extension of ETTs becomes critical and cannot be overlooked. Much literature aim to model and estimate the shape of extended targets [20]. Some algorithms represent the extension as a fixed shape, e.g., ellipse and rectangle [21], [22], while others can handle irregular shapes [23], [24]. In this paper, we do not estimate the shape but instead focus on the center state to reduce complexity. Moreover, due to the limitations of the standard measurement model [25], the point condensation before tracking is unnecessary.

A suitable tracking framework is also fundamental. Mainstream frameworks include: 1) Data association-based methods [26], e.g., joint probabilistic data association (JPDA) and multiple hypothesis tracking (MHT); 2) Random finite set (RFS)-based methods [27], e.g., probability hypothesis density (PHD) filter, cardinalized PHD (CPHD) filter, multi-Bernoulli (MB) filter, the generalized labeled MB (GLMB) filter [28] and the labeled MB (LMB) filter [29]. In dense and various ETT tracking scenarios, the accuracy of trajectories is quite important. The motivations for choosing extended target trajectory PHD (ET-TPHD) filter [30] in this paper are as follows: 1) Although we do not aim at the shape of ETTs, the ET-TPHD

This work was supported in part by the National Natural Science Foundation of China under Grant 62231008 and 62301127, in part by the China Postdoctoral Science Foundation under Grant BX20220057, 2023M730509 and GZB20230112, in part by the "Tianfu Qingcheng" Plan of Sichuan Province under Grant 1332 and 1395.

filter can cope their extension; 2) The TPHD filter is not only a filter but also a smoother can smooth and optimize historical trajectories; 3) The RFS-based ET-TPHD filter is efficient and flexible. The main contributions can be summarized as follows:

- Inspired by driving habits, we propose an interactive motion model to avoid collision when ETTs are neighboring. This model enhances sensor capability in distinguishing targets and mitigates trajectory confusion.
- To mitigate the impact of measurement noise, especially in scenarios where ETTs are far, we propose a lane constraint method. In this method, lanes are modeled as pseudo measurements, allowing for the constraint of ETTs through pseudo update.
- The interaction and constraint based on the ET-TPHD (IC-ET-TPHD) filter is realized for ETT tracking. The performance is assessed by simulation and experiment.

II. Background

A. Variables and notations of sets of trajectories

Let $\mathbf{x}_k \in \mathbb{X}$ be the single target state at time k where $\mathbb{X}$ denotes the space of single target state. In the context of traffic target tracking, we are interested in estimating the current state of traffic targets as well as their previous states. Consequently, trajectory, a sequence of target states that can start at any time step and have any length, is suitable for this application. Further, a single trajectory at time k is represented by $X_k = (t, \mathbf{x}^{1:o})$ where $\mathbf{x}^{1:o} = (\mathbf{x}^1, \ldots, \mathbf{x}^o)$ denotes a sequence of target states at consecutive time steps starting at time t with length o. At time k, a trajectory $X_k = (t, \mathbf{x}^{1:o})$ exists from time t to $t+o-1$, the variable $(t, o) \in \mathbb{O}_{(k)} = \{(t, o) : 0 \leq t \leq k, 1 \leq o \leq k-t+1\}$ and $X_k \in \mathbb{T}_{(k)} = \uplus_{(t,o)\in\mathbb{O}_{(k)}} \{t\} \times \mathbb{X}^o$ where $\uplus$ is the disjoint union [30].

Here, we consider that $\mathbf{x}_k = [p_{x,k}, v_{x,k}, p_{y,k}, v_{y,k}]^\top$ where '$\top$' is the matrix transpose operation, $p_{x,k}$ and $v_{x,k}$ denote the position and velocity in the x-direction, $p_{y,k}$ and $v_{y,k}$ denote the position and velocity in the y-direction so that $\mathbb{X} = \mathbb{R}^4$. We define the velocity vector of target i at time k

$$\vec{v}_k^i = v_{x,k}^i \vec{x} + v_{y,k}^i \vec{y}. \tag{1}$$

Let $\mathbf{X}_k = \{X_k^1, \ldots, X_k^{n_k}\} \in \mathcal{F}(\mathbb{T}_{(k)})$ denote the trajectory set at time k where n_k is the number of trajectories at time k and $\mathcal{F}(\mathbb{T}_{(k)})$ denotes the set of all finite subsets of $\mathbb{T}_{(k)}$.

B. Standard ET-TPHD filter

The adopted Poisson model for extended targets can be found in [25]. Let $D_{k|k-1}$ and D_k denote the prior and posterior intensities at time k, respectively. The prediction equation is given by [30]

$$D_{k|k-1} = D_{k|k-1}^{\mathrm{S}}(X) + D_k^{\beta}(X) \tag{2}$$

where the survival term and the newborn term respectively are

$$\begin{aligned} D_{k|k-1}^{\mathrm{S}}\left(t, \mathbf{x}^{1:o}\right) &= p_S(\mathbf{x}^{o-1}) f(\mathbf{x}^o|\mathbf{x}^{o-1}) \\ &\quad \times D_{k-1}(t, \mathbf{x}^{1:o-1}) 1_{\{k\}}(t+o-1), \\ D_k^{\beta}\left(t, \mathbf{x}^{1:o}\right) &= D_{\beta_\tau}(\mathbf{x}^1) 1_{\{k\}}(t) \end{aligned}$$

with $f(\cdot|\mathbf{x})$ the single target transition density, $p_S(\mathbf{x})$ the probability of survival, $\beta_\tau(\cdot)$ the Poisson multitarget density of newborn targets and the indicator function

$$1_A(z) = \begin{cases} 1, & z \in A \\ 0, & z \notin A \end{cases}. \tag{3}$$

The update equation is given by [25], [30]

$$D_k(X) = \left[D_k^{\mathrm{MD}}(X) + \sum_{\mathrm{p}\angle\mathbf{Z}_k} \sum_{\mathbf{W}\in\mathrm{p}} D_k^{\mathrm{D}}(X, \mathbf{W}) \right] 1_{\{k-o+1\}}(t) \tag{4}$$

where the missed detection term and the detection term are

$$D_k^{\mathrm{MD}}\left(t, \mathbf{x}^{1:o}\right) = \left(1 - \left(1 - e^{-\gamma(\mathbf{x}^o)}\right) p_D(\mathbf{x}^o)\right) D_{k|k-1}\left(t, \mathbf{x}^{1:o}\right),$$

$$\begin{aligned} D_k^{\mathrm{D}}\left(t, \mathbf{x}^{1:o}, \mathbf{W}\right) &= e^{-\gamma(\mathbf{x}^o)} p_D(\mathbf{x}^o) \times \sum_{\mathrm{p}\angle\mathbf{Z}_k} \omega_{\mathrm{p}} \sum_{\mathbf{W}\in\mathrm{p}} \frac{\gamma(\mathbf{x}^o)^{|\mathbf{W}|}}{d_{\mathbf{W}}} \\ &\quad \times \prod_{\mathbf{z}\in\mathbf{W}} \frac{g(\mathbf{z}|\mathbf{x}^o)}{\lambda_k c_k(\mathbf{z})} D_{k|k-1}\left(t, \mathbf{x}^{1:o}\right) \end{aligned}$$

with $g(\cdot|\mathbf{x})$ the measurement likelihood, $|\cdot|$ the cardinality of a set, $\gamma(\mathbf{x})$ the expected number of generated measurements, $p_D(\mathbf{x})$ the probability of detection, λ_k and $c_k(\cdot)$ are the mean number and spatial distribution of clutter at time k. The notation $\mathrm{p}\angle\mathbf{Z}_k$ indicates the partitioning of the measurement set $\mathbf{Z}_k = \{\mathbf{z}_k^1, \ldots, \mathbf{z}_k^{m_k}\}$ with m_k the number of measurements into non-empty cells $\mathbf{W}$ across all possible partitions. ω_{p} and $d_{\mathbf{W}}$, the normalization factors, are given by [25], [30]

$$\omega_{\mathrm{p}} = \frac{\prod_{\mathbf{W}\in\mathrm{p}} d_{\mathbf{W}}}{\sum_{\mathrm{p}'\angle\mathbf{Z}_k} \prod_{\mathbf{W}'\in\mathrm{p}'} d_{\mathbf{W}'}}, \tag{5}$$

$$\begin{aligned} d_{\mathbf{W}} &= \delta_{|\mathbf{W}|,1} \\ &\quad + \int e^{-\gamma(\mathbf{y})} \gamma(\mathbf{y})^{|\mathbf{W}|} p_D(\mathbf{y}) \prod_{\mathbf{z}\in\mathbf{W}} \frac{g(\mathbf{z}|\mathbf{y})}{\lambda_k c_k(\mathbf{z})} D_{k|k-1}(\mathbf{y}) d\mathbf{y} \end{aligned} \tag{6}$$

where $\delta_{i,j}$ is the the Kronecker delta and

$$D_{k|k-1}(\mathbf{y}) = \sum_{t=1}^{k} \int D_{k|k-1}\left(t, \mathbf{x}^{1:k-t}, \mathbf{y}\right) d\mathbf{x}^{1:k-t} \tag{7}$$

with the set integral on single trajectory space $\mathbb{T}_{(k)}$ [30]

$$\int D(X) dX = \sum_{(t,o)\in\mathbb{O}_{(k)}} \int D\left(t, \mathbf{x}^{1:o}\right) d\mathbf{x}^{1:o}. \tag{8}$$

III. The Proposed IC-ET-TPHD Filter for ETT Tracking

In this section, we propose the interactive motion model and the lane constraint method. On this basis, the implementation of the IC-ET-TPHD filter is detailed.

A. Interactive motion model for collision avoidance

When a vehicle travels on the road, its motion is typically influenced by neighboring vehicles to avoid collision. To determine whether there is interaction between targets in a rational way, the distance matrix at time k is defined by

$$\mathbf{D}_k = \left(d_k^{ij}\right)_{n_k \times n_k} \tag{9}$$

where d_k^{ij} is the Euclidean distance between target i and target j at time k. Therefore, the interactive motion model can be written as

$$\mathbf{x}_{k+1}^i = \tilde{\mathbf{F}}_k^i \mathbf{x}_k^{\text{aug}} + \mathbf{v}_k \tag{10}$$

where $\mathbf{x}_k^{\text{aug}} = [\mathbf{x}_k^{1,\top}, \dots, \mathbf{x}_k^{n_k,\top}]^\top$ is the augmented state vector consisted of all target states at time k, and $\mathbf{v}_k$ is the Gaussian process noise vector with zero mean and covariance

$$\mathbf{Q} = \mathbf{\Gamma} \begin{bmatrix} \sigma_x^2 & 0 \\ 0 & \sigma_y^2 \end{bmatrix} \mathbf{\Gamma}^\top, \text{ where } \mathbf{\Gamma} = \begin{bmatrix} \frac{T_s^2}{2} & T_s & 0 & 0 \\ 0 & 0 & \frac{T_s^2}{2} & T_s \end{bmatrix}^\top, \tag{11}$$

T_s is the sampling interval, σ_x, σ_y are the standard deviations of acceleration in the x and y directions, respectively. Besides, the interactive motion function of target i at time k is

$$\tilde{\mathbf{F}}_k^i = \left[\mathbf{F}_k^{i1}, \dots, \mathbf{F}_k^{ii}, \dots, \mathbf{F}_k^{in_k}\right] \tag{12}$$

where $\mathbf{F}_k^{ii}$ is the preset motion model. Moreover, according to the distance between target i and target j ($i \neq j$),

$$\mathbf{F}_k^{ij} = \begin{cases} \mathbf{0}_{4,4}, & d_k^{ij} > \phi \\ \begin{bmatrix} \alpha_k^{ij} & 0 \\ 0 & \beta_k^{ij} \end{bmatrix} \otimes \begin{bmatrix} 0 & T_s \\ 0 & 1 \end{bmatrix}, & d_k^{ij} \leq \phi \end{cases} \tag{13}$$

where $\mathbf{0}_{i,j}$ is the $i \times j$ zero matrix, '$\otimes$' is the Kronecker product, ϕ is the threshold deciding whether the target interact with each other, α_k^{ij} and β_k^{ij} are the interactive factors at time k of target j on target i in x- and y-direction, respectively. Obviously, there is an interaction force of target j on target i only when $d_k^{ij} \leq \phi$. Moreover, the interactive motion function $\mathbf{F}_k^{ij}$ resulting from the interaction force is detailed below.

Firstly, the interactive direction matrix $\mathbf{L}_k$ and vector $\vec{l}_k^{ij}$ at time k are defined by

$$\mathbf{L}_k = \left(\vec{l}_k^{ij}\right)_{n_k \times n_k}, \vec{l}_k^{ij} = \frac{(p_{x,k}^j - p_{x,k}^i)\vec{x} + (p_{y,k}^j - p_{y,k}^i)\vec{y}}{\sqrt{(p_{x,k}^j - p_{x,k}^i)^2 + (p_{y,k}^j - p_{y,k}^i)^2}}. \tag{14}$$

It is remarkable that $|\vec{l}_k^{ij}| = 1$ with $|\cdot|$ the norm operator, and the interactive direction vector $\vec{l}_k^{ij}$ points from target i to target j, indicating the direction of the potential interaction force of target j on target i.

Then, the magnitude matrix $\mathbf{A}_k$ at time k is defined by

$$\mathbf{A}_k = \left(a_k^{ij}\right)_{n_k \times n_k} \quad \text{where} \quad a_k^{ij} = \vec{v}_k^i \cdot \vec{l}_k^{ij} \tag{15}$$

is the magnitude of the velocity $\vec{v}_k^i$ along the direction $\vec{l}_k^{ij}$. As a basis for whether there is interaction between target i and target j except $\mathbf{D}_k$, a_k^{ij} denotes the magnitude of the velocity of target i along the direction $\vec{l}_k^{ij}$.

Besides, the interaction force matrix at time k is defined by

$$\mathbf{B}_k = \left(\vec{b}_k^{ij}\right)_{n_k \times n_k} \tag{16}$$

where $\vec{b}_k^{ij}$ is the interaction force of target j on target i and is calculated by

$$\vec{b}_k^{ij} = \begin{cases} a_k^{ji}\vec{l}_k^{ij}, & a_k^{ij} > 0, \dfrac{d_k^{ij}}{a_k^{ij} + a_k^{ji}} > 0 \\ 0, & \text{otherwise} \end{cases}. \tag{17}$$

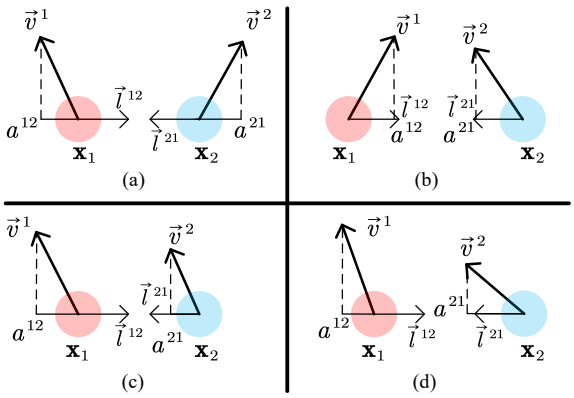

Fig. 1. Schematic diagram of interaction force.

The interaction force is reflected as the repulsive force. $\vec{b}_k^{ij}$ in (17) is in terms of a_k^{ji} which shows that the repulsive force of target j on target i depends on the velocity of target j. An example with four cases is given in Fig. 1, omitting the time stamp, there are two neighboring targets $\mathbf{x}_1$, $\mathbf{x}_2$ whose distance $d^{12} = d^{21} < \phi$. The interaction decision is as follows. Note that this is not the particular case of x-direction, but the common case and the interaction force is put on the direction of the connection.

Case	Magnitude	Criterion	Interaction force
(a)	$a^{12} < 0, a^{21} < 0$	$d^{12}/(a^{12} + a^{21}) < 0$	$\vec{b}^{12} = 0, \vec{b}^{21} = 0$
(b)	$a^{12} > 0, a^{21} > 0$	$d^{12}/(a^{12} + a^{21}) > 0$	$\vec{b}^{12} \neq 0, \vec{b}^{21} \neq 0$
(c)	$a^{12} < 0, a^{21} > 0$	$d^{12}/(a^{12} + a^{21}) < 0$	$\vec{b}^{12} = 0, \vec{b}^{21} = 0$
(d)	$a^{12} < 0, a^{21} > 0$	$d^{12}/(a^{12} + a^{21}) > 0$	$\vec{b}^{12} = 0, \vec{b}^{21} \neq 0$

Lastly, after calculating the matrix $\mathbf{L}_k$, $\mathbf{A}_k$ and $\mathbf{B}_k$ step by step, we can obtain

$$\alpha_k^{ij} = \eta \cdot \mathfrak{X}(\vec{b}_k^{ij}), \quad \beta_k^{ij} = \eta \cdot \mathfrak{Y}(\vec{b}_k^{ij}), \tag{18}$$

where $\eta \geq 0$ is the scale factor and the operators

$$\mathfrak{X}(a\vec{x} + b\vec{y}) = a, \quad \mathfrak{Y}(a\vec{x} + b\vec{y}) = b. \tag{19}$$

B. Lane constraint via pseudo update

When a vehicle travels on the road, its motion is influenced not only by neighboring vehicles but also by road information. A typical example is that drivers often keep their cars in the middle of the lane, with lane change behaviors being infrequent, rapid, and brief. Lanes can thus be considered as prior information to leverage and improve the performance of the filter.

As illustrated in Fig. 2, there are two parallel lanes of width M whose center x coordinates are L_1 and L_2, respectively. Besides, their are two vehicles at time $k-1$, marked with stars, whose posterior states are

$$\mathbf{x}_{k-1}^1 \sim \mathcal{N}(\cdot; \mathbf{m}_{k-1}^1, \mathbf{P}_{k-1}^1), \tag{20a}$$

$$\mathbf{x}_{k-1}^2 \sim \mathcal{N}(\cdot; \mathbf{m}_{k-1}^2, \mathbf{P}_{k-1}^2) \tag{20b}$$

where $\mathcal{N}(\cdot; \mathbf{m}, \mathbf{P})$ denotes a Gaussian density with mean $\mathbf{m}$ and covariance $\mathbf{P}$. Here, we only consider the current state while the trajectory version is detailed in the Section III-C.

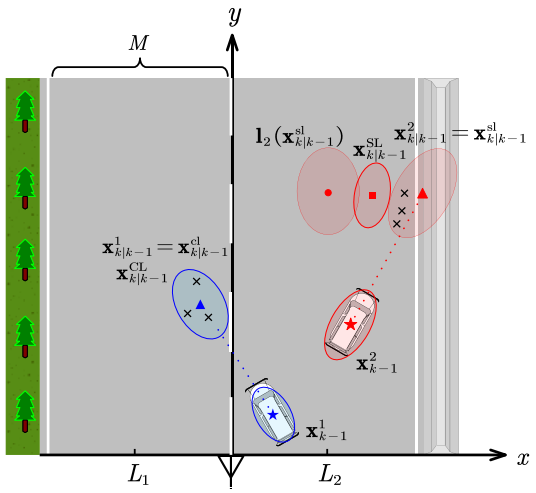

Fig. 2. Schematic diagram of lane constraint.

1) Lane change trend judgment

To determine whether the target should be constrained by the lane, their prior states are

$$\mathbf{x}^1_{k|k-1} \sim \mathcal{N}(\cdot;\mathbf{m}^1_{k|k-1},\mathbf{P}^1_{k|k-1}), \tag{21a}$$
$$\mathbf{x}^2_{k|k-1} \sim \mathcal{N}(\cdot;\mathbf{m}^2_{k|k-1},\mathbf{P}^2_{k|k-1}) \tag{21b}$$

according to the interactive motion model mentioned in Section III-A. Then, once we obtain the prediction of targets, a gating operation is executed to judge whether each target intends to change lanes or not. A simple but intuitive way is to firstly calculate the Mahalanobis distance of measurements (i.e., black forks in Fig. 2) and the prediction state (i.e., triangles in Fig. 2)

$$\mathbf{E}_k = \left(e^{ij}_k\right)_{m_k\times n_{k-1}} \tag{22}$$
$$e^{ij}_k = \left(\mathbf{z}^j_k - \mathbf{z}^i_{k|k-1}\right)^\top \mathbf{S}^{-1}_k \left(\mathbf{z}^j_k - \mathbf{z}^i_{k|k-1}\right) \tag{23}$$

where $\mathbf{z}^i_{k|k-1}$ and $\mathbf{S}_k$ can be calculated by measurement function.

Then, the association matrix $\mathbf{G}_k$ and the association indicator g^{ij}_k at time k are defined by

$$\mathbf{G}_k = \left(g^{ij}_k\right)_{m_k\times n_{k-1}}, \quad g^{ij}_k = \begin{cases} 1, & e^{ij}_k < \psi \\ 0, & e^{ij}_k \geq \psi \end{cases} \tag{24}$$

where ψ is the gating threshold. Accordingly, we can judge whether each target at time $k-1$ has a tendency to change lanes at time k with $\mathbf{G}_k$. Here, we define the judgement matrix

$$\mathbf{U}_k = \left(u^{ij}_k\right)_{m_k\times n_{k-1}} \tag{25}$$

where the indicator

$$u^{ij}_k = \begin{cases} 1, & g^{ij}_k = 1, \epsilon^{ij}_k = 1 \\ 0, & \text{otherwise} \end{cases} \tag{26}$$

with the lane indicator

$$\epsilon^{ij}_k = \begin{cases} 1, & \text{measurement } i \text{ and target } j \\ & \text{are in different lanes} \\ 0, & \text{otherwise} \end{cases}. \tag{27}$$

Finally, the lane change vector can be defined by

$$\boldsymbol{\chi}_k = \left[\chi^1_k, \ldots, \chi^{n_{k-1}}_k\right] \tag{28}$$

where the trend indicator

$$\chi^j_k = \begin{cases} 1, & \sum_{i=1}^{m_k} u^{ij}_k \geq \sum_{i=1}^{m_k} g^{ij}_k \Big/ 2 \\ 0, & \text{otherwise} \end{cases} \tag{29}$$

means that if more than half of the associated measurements of the target are not in the same lane as the target, the target is considered to have a trend to change lanes (i.e., $\chi^j_k = 1$). In Fig. 2, target 1, tagged as cl, intends to change lanes while target 2, tagged as sl, does not, and (21) can be rewritten as

$$\mathbf{x}^{\mathrm{cl}}_{k|k-1} \sim \mathcal{N}(\cdot;\mathbf{m}^{\mathrm{cl}}_{k|k-1},\mathbf{P}^{\mathrm{cl}}_{k|k-1}), \tag{30a}$$
$$\mathbf{x}^{\mathrm{sl}}_{k|k-1} \sim \mathcal{N}(\cdot;\mathbf{m}^{\mathrm{sl}}_{k|k-1},\mathbf{P}^{\mathrm{sl}}_{k|k-1}). \tag{30b}$$

2) Pseudo measurements of lanes

Since target 2 does not intend to change lanes, a pseudo measurement of lane 2, marked with red dot in Fig. 2, based on its state is generated by

$$\mathbf{l}_2(\mathbf{x}^{\mathrm{sl}}_{k|k-1}) \sim \mathcal{N}(\cdot;\mathbf{m}^{l}_{k|k-1},\mathbf{P}^{l}_{k|k-1}) \quad \text{where} \tag{31}$$

$$\mathbf{m}^{l}_{k|k-1} = \left[L_2, \mu\cdot\mathbf{m}^{\mathrm{sl}}_{k|k-1}(2), \mathbf{m}^{\mathrm{sl}}_{k|k-1}(3), \mathbf{m}^{\mathrm{sl}}_{k|k-1}(4)\right]^\top,$$
$$\mathbf{P}^{l}_{k|k-1} = \mathrm{blkdiag}\left([(M/3)^2, \mathbf{P}^{\mathrm{sl}}_{k|k-1}(2:4,2:4)]\right)$$

with $\mu \leq 0$ the decay factor dragging the target towards the lane center. Here, $\mathbf{m}(i)$ is the ith element of the vector $\mathbf{m}$ and $\mathbf{P}(a:b,c:d)$ is the submatrix, consisted of the $a\sim b$ rows and $c\sim d$ columns of the matrix $\mathbf{P}$. It is significant that the value $M/3$ is according to 3σ criterion.

3) Pseudo update using the pseudo measurements of lanes

A pseudo update step is performed to constrain the targets that do not intend to change lanes, approaching to the middle of the same lane. The targets after pseudo update are

$$\mathbf{x}^1_{k|k-1} \sim \mathcal{N}(\cdot;\mathbf{m}^{\mathrm{CL}}_{k|k-1},\mathbf{P}^{\mathrm{CL}}_{k|k-1}), \tag{32a}$$
$$\mathbf{x}^2_{k|k-1} \sim \mathcal{N}(\cdot;\mathbf{m}^{\mathrm{SL}}_{k|k-1},\mathbf{P}^{\mathrm{SL}}_{k|k-1}) \tag{32b}$$

where the mean and covariance of target 1 are fixed, that is

$$\mathbf{m}^{\mathrm{CL}}_{k|k-1} = \mathbf{m}^{\mathrm{cl}}_{k|k-1}, \quad \mathbf{P}^{\mathrm{CL}}_{k|k-1} = \mathbf{P}^{\mathrm{cl}}_{k|k-1}.$$

However, the mean and covariance of target 2 after pseudo update, marked with red square in Fig. 2, are

$$\mathbf{m}^{\mathrm{SL}}_{k|k-1} = \mathbf{m}^{\mathrm{sl}}_{k|k-1} + \mathbf{P}^{\mathrm{sl}}_{k|k-1}\tilde{\mathbf{H}}^\top\tilde{\mathbf{S}}^{-1}\left(\mathbf{m}^{l}_{k|k-1} - \mathbf{m}^{\mathrm{sl}}_{k|k-1}\right),$$
$$\mathbf{P}^{\mathrm{SL}}_{k|k-1} = \left(\mathbf{I}_4 - \mathbf{P}^{\mathrm{sl}}_{k|k-1}\tilde{\mathbf{H}}^\top\tilde{\mathbf{S}}^{-1}\tilde{\mathbf{H}}\right)\mathbf{P}^{\mathrm{sl}}_{k|k-1} \tag{33}$$

where all the parameters can be calculated by Kalman filter

$$\tilde{\mathbf{S}} = \tilde{\mathbf{H}}\mathbf{P}^{\mathrm{sl}}_{k|k-1}\tilde{\mathbf{H}}^\top + \mathbf{P}^{l}_{k|k-1}, \quad \tilde{\mathbf{H}} = \mathbf{I}_4.$$

where $\mathbf{I}_i$ is the identity matrix of dimension i.

C. The proposed IC-ET-TPHD filter

In this part, we realize the interactive motion model and lane constraint method based on the ET-TPHD filter mentioned in Section II-B. Moreover, Gaussian mixture (GM) approximation [31] is adopted as the implementation tool because it is convenient to be embedded with other models and methods.

We firstly define the trajectory Gaussian density [30]

$$\mathcal{N}\left(t,\mathbf{x}^{1:o};t_k,\mathbf{m}_k,\mathbf{P}_k\right)=\begin{cases}\mathcal{N}(\mathbf{x}^{1:o};\mathbf{m}_k,\mathbf{P}_k), & t=t_k,o=o_k\\ 0, & \text{otherwise}\end{cases} \tag{34}$$

where $o_k=\dim(\mathbf{m}_k)/d_x$ is the duration with $d_x=4$ the dimension of target state, t_k is the start time, $\mathbf{m}_k\in\mathbb{R}^{4\cdot o_k}$ is the mean and $\mathbf{P}_k\in\mathbb{R}^{4\cdot o_k\times 4\cdot o_k}$ is the covariance. We hold the assumption that the expected number of generated measurements, the target survival and detection probabilities are constant, i.e.,

$$\gamma(\mathbf{x})=\gamma,\quad p_S(\mathbf{x})=p_S,\quad p_D(\mathbf{x})=p_D. \tag{35}$$

1) The prediction of IC-ET-TPHD filter

Suppose the posterior intensity at time $k-1$ is a trajectory GM of the form

$$D_{k-1}(X)=\sum_{i=1}^{J_{k-1}}w_{k-1}^{i}\mathcal{N}\left(X;t_{k-1}^{i},\mathbf{m}_{k-1}^{i},\mathbf{P}_{k-1}^{i}\right) \tag{36}$$

where $t_{k-1}^{i}+o_{k-1}^{i}-1=k-1$. The prior intensity at time k is also a trajectory GM of the form where the newborn term is obtained by track initiation and the survival term in (2) is

$$D_{k|k-1}^{\mathrm{S}}(X)=\sum_{i=1}^{J_{k-1}}w_{k|k-1}^{i}\mathcal{N}\left(X;t_{k|k-1}^{i},\mathbf{m}_{k|k-1}^{i},\mathbf{P}_{k|k-1}^{i}\right) \tag{37}$$

and

$$\begin{aligned}w_{k|k-1}^{i}&=p_S w_{k-1}^{i},\quad t_{k|k-1}^{i}=t_{k-1}^{i},\\ \mathbf{m}_{k|k-1}^{i}&=\left[\mathbf{m}_{k-1}^{i,\top},\left(\tilde{\mathbf{F}}_{k-1}^{i}\mathbf{m}_{k-1}^{\mathrm{aug}}\right)^{\top}\right]^{\top},\\ \mathbf{P}_{k|k-1}^{i}&=\begin{bmatrix}\mathbf{P}_{k-1}^{i} & \mathbf{P}_{k-1}^{\mathrm{aug}}\tilde{\mathbf{F}}_{k-1}^{i,\top}\\ \tilde{\mathbf{F}}_{k-1}^{i}\mathbf{P}_{k-1}^{\mathrm{aug}} & \tilde{\mathbf{F}}_{k-1}^{i}\mathbf{P}_{k-1}^{\mathrm{aug}}\tilde{\mathbf{F}}_{k-1}^{i,\top}+\mathbf{Q}\end{bmatrix}\end{aligned}$$

with $\tilde{\mathbf{F}}_{k-1}^{i}$ the interactive motion function in (12) while

$$\mathbf{F}_{k-1}^{ii}=\left[\mathbf{0}_{2,o_{k-1}^{i}-1},\mathbf{I}_2\right]\otimes\begin{bmatrix}1 & T_s\\ 0 & 1\end{bmatrix}\quad\text{and}$$

$$\mathbf{F}_{k-1}^{ij}=\begin{cases}\mathbf{0}_{4,o_{k-1}^{j}}, & d_k^{ij}>\phi\\ \left[\mathbf{0}_{2,o_{k-1}^{j}-1},\begin{bmatrix}\alpha_k^{ij} & 0\\ 0 & \beta_k^{ij}\end{bmatrix}\right]\otimes\begin{bmatrix}0 & T_s\\ 0 & 1\end{bmatrix}, & d_k^{ij}\le\phi\end{cases}$$

because the target is in the form of trajectory rather than current state in Section III-A. Here, the constant velocity model is adopted. However, the preset motion model can be generalized to other more complex motion models [32]. Besides, the augmented components

$$\begin{aligned}\mathbf{m}_{k-1}^{\mathrm{aug}}&=\left[\mathbf{m}_{k-1}^{1,\top},\ldots,\mathbf{m}_{k-1}^{J_{k-1},\top}\right]^{\top},\\ \mathbf{P}_{k-1}^{\mathrm{aug}}&=\mathrm{blkdiag}\left(\left[\mathbf{P}_{k-1}^{1},\ldots,\mathbf{P}_{k-1}^{J_{k-1}}\right]\right).\end{aligned}$$

2) The pseudo update of IC-ET-TPHD filter

Suppose the prior intensity at time k is a trajectory GM of the form

$$D_{k|k-1}(X)=\sum_{i=1}^{J_{k|k-1}}w_{k|k-1}^{i}\mathcal{N}\left(X;t_{k|k-1}^{i},\mathbf{m}_{k|k-1}^{i},\mathbf{P}_{k|k-1}^{i}\right). \tag{38}$$

According to the lane change vector $\boldsymbol{\chi}_k$ in Section III-B, the pseudo update intensity $D_{k|k-1}(X)$ can be divided into

$$D_{k|k-1}(X)=D_{k|k-1}^{\mathrm{sl}}(X)+D_{k|k-1}^{\mathrm{cl}}(X) \tag{39}$$

where $D_{k|k-1}^{\mathrm{sl}}(X)$ and $D_{k|k-1}^{\mathrm{cl}}(X)$ denote the stay lane term and the change lanes term, respectively. Furthermore,

$$D_{k|k-1}^{\mathrm{sl}}(X)=\sum_{i=1}^{J_{k|k-1}^{\mathrm{sl}}}w_{k|k-1}^{\mathrm{sl},i}\mathcal{N}\left(X;t_{k|k-1}^{\mathrm{sl},i},\mathbf{m}_{k|k-1}^{\mathrm{sl},i},\mathbf{P}_{k|k-1}^{\mathrm{sl},i}\right). \tag{40}$$

Then, the pseudo update intensity at time k is also a trajectory GM of the form

$$D_{k|k-1}^{*}(X)=D_{k|k-1}^{\mathrm{SL}}(X)+D_{k|k-1}^{\mathrm{CL}}(X) \tag{41}$$

where the change lanes term $D_{k|k-1}^{\mathrm{CL}}(X)=D_{k|k-1}^{\mathrm{cl}}(X)$ and the stay lane term after pseudo update is

$$D_{k|k-1}^{\mathrm{SL}}(X)=\sum_{i=1}^{J_{k|k-1}^{\mathrm{SL}}}w_{k|k-1}^{\mathrm{SL},i}\mathcal{N}\left(X;t_{k|k-1}^{\mathrm{SL},i},\mathbf{m}_{k|k-1}^{\mathrm{SL},i},\mathbf{P}_{k|k-1}^{\mathrm{SL},i}\right) \tag{42}$$

with

$$J_{k|k-1}^{\mathrm{SL}}=J_{k|k-1}^{\mathrm{sl}},\ w_{k|k-1}^{\mathrm{SL},i}=w_{k|k-1}^{\mathrm{sl},i},\ t_{k|k-1}^{\mathrm{SL},i}=t_{k|k-1}^{\mathrm{sl},i},$$

and $\mathbf{m}_{k|k-1}^{\mathrm{SL},i}$, $\mathbf{P}_{k|k-1}^{\mathrm{SL},i}$ are given in (33) while

$$\tilde{\mathbf{H}}_i=\left[\mathbf{0}_{1,o_{k|k-1}^{i}-1},1\right]\otimes\mathbf{I}_4$$

because the target is in the form of trajectory rather than current state in Section III-B.

3) The update of IC-ET-TPHD filter

Suppose the prior intensity after pseudo update at time k is a trajectory GM of the form

$$D_{k|k-1}^{*}(X)=\sum_{i=1}^{J_{k|k-1}}w_{k|k-1}^{i}\mathcal{N}\left(X;t_{k|k-1}^{i},\mathbf{m}_{k|k-1}^{*,i},\mathbf{P}_{k|k-1}^{*,i}\right). \tag{43}$$

Then, the posterior intensity at time k is also a trajectory GM of the form where the missed detection term $D_k^{\mathrm{MD}}(X)$ in (4) is the same as the prior term except the weights

$$w_k^{i}=\left(1-\left(1-e^{-\gamma}\right)p_D\right)w_{k|k-1}^{i}$$

and the detection term in (4) is

$$D_{k|k-1}^{\mathrm{D}}(X,\mathbf{W})=\sum_{i=1}^{J_{k|k-1}}w_k^{i,\mathbf{W}}\mathcal{N}\left(X;t_k^{i,\mathbf{W}},\mathbf{m}_k^{i,\mathbf{W}},\mathbf{P}_k^{i,\mathbf{W}}\right). \tag{44}$$

where $t_k^{i,\mathbf{W}} = t_{k|k-1}^i$,

$$w_k^{i,\mathbf{W}} = \frac{\omega_{\mathrm{p}}}{d_{\mathbf{W}}} e^{-\gamma}\gamma^{|\mathbf{W}|} p_D \prod_{\mathbf{z}\in\mathbf{W}} \frac{g(\mathbf{z}|\mathbf{m}_{k|k-1}^{*,i})}{\lambda_k c_k(\mathbf{z})},$$
$$\mathbf{m}_k^{i,\mathbf{W}} = \mathbf{m}_{k|k-1}^{*,i} + \mathbf{K}_k^i\left(\mathbf{z}^{\mathbf{W}} - \mathbf{1}_{|\mathbf{W}|,1} \otimes \mathbf{z}_{k|k-1}^i\right),$$
$$\mathbf{P}_k^{i,\mathbf{W}} = \mathbf{P}_{k|k-1}^{*,i} - \mathbf{K}_k^i \mathbf{S}_k^i \mathbf{K}_k^{i,\top}$$

with ω_{p} given in (5) and

$$g(\mathbf{z}|\mathbf{m}_{k|k-1}^{*,i}) = \mathcal{N}\left(\mathbf{z}; \mathbf{z}_{k|k-1}^i, \mathbf{S}_k^i\right),\ \mathbf{z}^{\mathbf{W}} = \left[\mathbf{z}_1^\top, \ldots, \mathbf{z}_{|\mathbf{W}|}^\top\right]^\top,$$
$$d_{\mathbf{W}} = \delta_{|\mathbf{W}|,1} + \sum_{i=1}^{J_{k|k-1}} e^{-\gamma}\gamma^{|\mathbf{W}|} p_D \prod_{\mathbf{z}\in\mathbf{W}} \frac{g(\mathbf{z}|\mathbf{m}_{k|k-1}^{*,i})}{\lambda_k c_k(\mathbf{z})} w_{k|k-1}^i.$$

Usually, due to the non-linear measurement model and the augmentation of trajectories, the parameters $\mathbf{z}_{k|k-1}^i$, $\mathbf{K}_k^i$ and $\mathbf{S}_k^i$ can be calculated by the singular value decomposition (SVD)-based unscented Kalman filter (UKF) [33] to avoid the issues of non-positive definite matrix and non-linear model.

D. Summary

To alleviate the computation load, the pruning, merging and capping operations are also adopted like [31]. As time progresses, the lengths of trajectories increase so that it is infeasible to implement. Consequently, the L-scan version of the IC-ET-TPHD filter is adopted like [30], but we omit its formulas here because of the space constraints.

IV. Performance Evaluation

In this section, to compare the tracking performance of the proposed IC-ET-TPHD filter and the standard algorithms comprehensively, the elaborate simulation scenarios and the experimental data from traffic frequency modulated continuous wave (FMCW) radar are processed.

A. Simulation results

As illustrated in Fig. 3 (a) and (b), there are four lanes of width 3.5m whose center x coordinates are $[-5.25, -1.75, 1.75, 5.25]$m in a $[-10, 10]\mathrm{m} \times [20, 200]\mathrm{m}$ traffic scenario involving 3 and 4 vehicles, respectively. Each vehicle contains 5 measurement sources within a rectangle 3.5×1.5m with detection probability $p_D = 1$ and survival probability $p_S = 0.99$. The sampling interval $T_s = 0.1$s and the duration is 10s. The standard deviations of the process noise $\sigma_x = \sigma_y = 10\mathrm{m/s}^2$. The non-linear measurement model of FMCW radar [34] is considered

$$\mathbf{z}_k = \mathbf{H}(\mathbf{x}_k) + \mathbf{w}_k \tag{45}$$

where the measurement vector $\mathbf{z}_k$ is in terms of range, radial velocity, bearing, and the non-linear measurement function is

$$\mathbf{H}(\mathbf{x}_k) = \begin{bmatrix} \sqrt{p_{x,k}^2 + p_{y,k}^2} \\ \dfrac{p_{x,k}v_{x,k} + p_{y,k}v_{y,k}}{\sqrt{p_{x,k}^2 + p_{y,k}^2}} \\ \arctan\left(p_{x,k}/p_{y,k}\right) \end{bmatrix}, \tag{46}$$

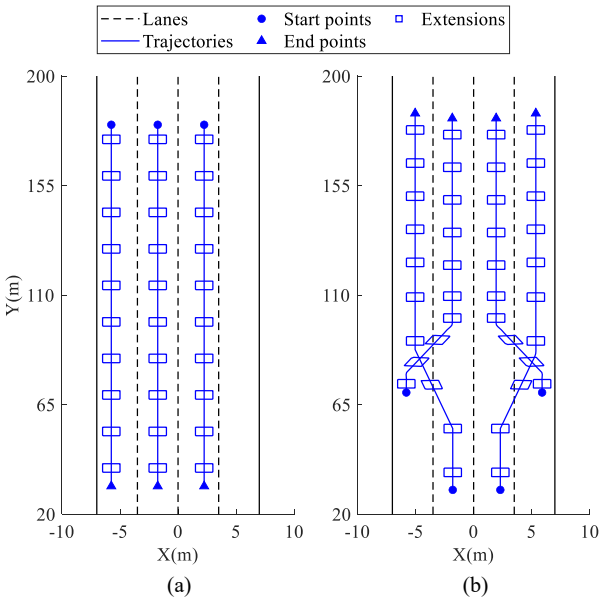

Fig. 3. The scenario and ground truth of two simulations. Their extensions are plotted every 10 time steps. (a) Simulation 1; (b) Simulation 2.

and $\mathbf{w}_k$ is the Gaussian measurement noise vector with zero mean and covariance $\mathbf{R} = q^2 \cdot \mathrm{diag}([1, 1, 0.005])^2$. The other algorithm parameters are the same as experiments shown in Table II. The proposed IC-ET-TPHD filter is evaluated along with the ET-TPHD filter and the JPDA filter [35], and the optimal sub-pattern assignment (OSPA) error [36] with parameters $c = 2$ and $p = 1$ is computed to compare the performance. The average OSPA errors over all time steps, under different measurement noise intensity q and clutter rate λ, are summarized in Table I for both Simulation 1 and 2. The numbers are averaged over 100 Monte Carlo runs.

1) Simulation 1

As shown in Fig. 3 (a), it is an intractable scenario with three neighboring vehicles coming together. Due to the spatial proximity, it is difficult for the clustering algorithm [37], [38] to distinguish the measurements of three vehicles. Thus, the JPDA filter certainly will blur them and confuse their trajectories. However, the ET-TPHD filter has better performance due to the RFS framework and the extended target model. Besides, the IC-ET-TPHD filter is superior with consideration of interactive motion and lane constraint. As shown in Table I, the OSPA error of the IC-ET-TPHD filter is the smallest while that of the JPDA filter is the largest with almost all parameters. With the increase of measurement noise density q or clutter rate λ, the performances of the filters deteriorate.

2) Simulation 2

As shown in Fig. 3 (b), it is an elaborate scenario with four leaving vehicles to test the change lanes case. The general results are similar to Simulation 1. As the scenario becomes difficult, the IC-ET-TPHD filter is less affected by clutter and measurement noise, and the superiority of the IC-ET-TPHD

TABLE I
AVERAGE OSPA ERRORS (M) OVER ALL TIME STEPS FOR DIFFERENT SIMULATION PARAMETERS: q AND λ.

(q, λ)	Simulation 1			Simulation 2		
	IC-ET-TPHD	ET-TPHD	JPDA	IC-ET-TPHD	ET-TPHD	JPDA
$(1, 10)$	0.435	0.778	0.754	0.724	0.890	0.858
$(2, 10)$	0.557	0.770	1.232	0.701	0.922	0.891
$(4, 10)$	0.589	0.986	1.261	0.742	0.964	1.072
$(2, 20)$	0.559	0.779	1.250	0.732	0.931	0.933
$(2, 30)$	0.561	0.803	1.252	0.737	0.935	0.953

TABLE II
THE PARAMETERS OF SCENARIO AND ALGORITHM

Parameter	**Value**	**Parameter**	**Value**
Sampling interval T_s	50ms	Range of ρ	$0 \sim 200$m
Process noise σ_x, σ_y	10m/s^2	Range of $v_\perp$	$-20 \sim 20$m/s
Survival probability p_S	0.99	Range of θ	$-\pi/2 \sim \pi/2$
Detection probability p_D	0.98	Clutter rate λ	20
The expected number of generated measurements γ	3	Measurement noise σ_ρ, σ_v, σ_θ	3m, 1.5m/s, 0.5°
Lane width M	3.5m	Threshold ϕ, ψ	8m, 5
Decay factor μ	-0.5	L-scan	5
Scale factor η	0.5		

filter is highlighted. In addition, the extension of neighboring vehicles are also addressed with the IC-ET-TPHD filter. Thus, the proposed IC-ET-TPHD filter can handle the neighboring vehicles change lanes when the measurement noise is large.

B. Experimental results

The parameters of scenario and algorithm are listed in Table II. To relieve the impact of numerous zero-Doppler clutter (e.g., green belts and fences) and compare the algorithm performance directly, the moving and static target separation strategy [34] is adopted. The details of two experiments and results are shown below.

1) Experiment 1

As shown in Fig. 4 (a), there are four longitudinal coming lanes whose center x coordinates are $[-5, -1.5, 2, 5.5]$m with trees and piers along the road in Experiment 1. It can be seen from Fig. 4 (b)-(d) that static clutter on both sides of the road is filtered out. Moreover, almost all the vehicles within the scenario can be detected and tracked except two neighboring trucks on the left. The ET-TPHD filter missed the left truck due to the proximity and the JPDA filter estimates the two trucks are in a tangle, but the IC-ET-TPHD filter can distinguish them well. The superiority of the proposed IC-ET-TPHD filter is also demonstrated by comparing the lateral error, especially when the vehicles change lanes or are neighboring. The error of common JPDA filter is significant while the ET-TPHD filter is more robust especially when the interaction and constraint are considered. Additionally, it is remarkable that the algorithm framework of RFS-based PHD filter is more efficient that JPDA filter from Fig. 4 (c) and (d).

2) Experiment 2

(a)

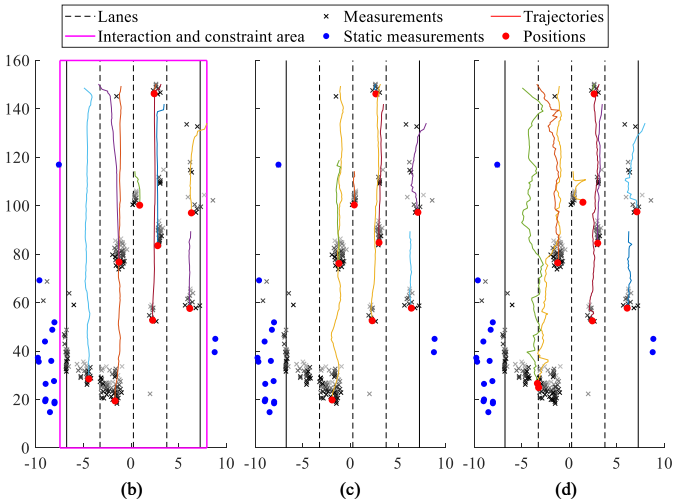

Fig. 4. The image of Experiment 1 and the tracking results of each algorithms. A grayscale is used to denote different time steps of measurements. (a) Experiment 1 image; (b) IC-ET-TPHD; (c) ET-TPHD; (d) JPDA.

As shown in Fig. 5 (a), there are three longitudinal coming lanes, three longitudinal leaving lanes and some static trees in Experiment 2. The center x coordinates of the six lanes from left to right are $[-3.5, 0, 3.5, 10.5, 14, 17.5]$m. Different from Experiment 1, the main error is caused by measurement noise rather than process noise since this is an expressway scenario and most vehicles are distinguished. Similarly, in Fig. 5 (b)-(d), all the vehicles can be detected and tracked but the IC-ET-TPHD is more accurate because the measurement noise is eliminated greatly with consideration of lane constraint.

V. CONCLUSION

This paper proposes a novel ET-TPHD filter that incorporates interactive motion and lane constraint to improve the tracking performance of ETTs when they are neighboring and dense. The proposed interactive motion model calculates indices to derive interaction forces aimed at collision avoidance. Additionally, lanes are modeled as pseudo measurements, enabling the incorporation of lane constraint through pseudo update. On this basis, the novel IC-ET-TPHD filter is developed, and its performance is evaluated through simulation and experiment, comparing it with standard algorithms.

REFERENCES

[1] H. Huang, A. V. Savkin, and C. Huang, "Decentralized autonomous navigation of a UAV network for road traffic monitoring," *IEEE Trans. Aerosp. Electron. Syst.*, vol. 57, no. 4, pp. 2558–2564, 2021.

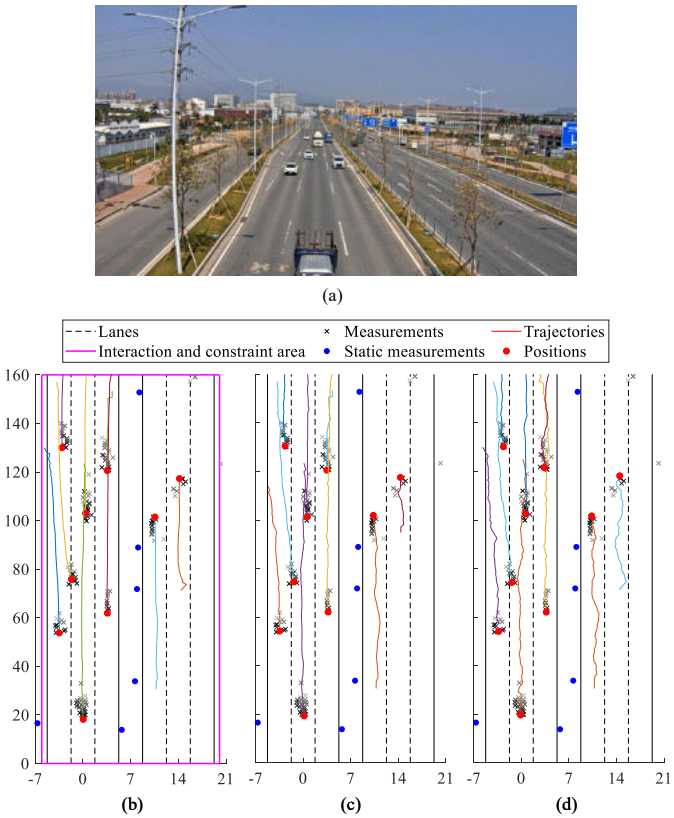

Fig. 5. The image of Experiment 2 and the tracking results of each algorithms. A grayscale is used to denote different time steps of measurements. (a) Experiment 2 image; (b) IC-ET-TPHD; (c) ET-TPHD; (d) JPDA.

[2] L. Chen and C. Englund, "Cooperative intersection management: A survey," *IEEE Trans. Intell. Transp. Syst.*, vol. 17, no. 2, pp. 570–586, 2015.

[3] X. Zhang, S. Hu, H. Zhang, and X. Hu, "A real-time multiple vehicle tracking method for traffic congestion identification," *KSII Trans. Internet Inf. Syst.*, vol. 10, no. 6, 2016.

[4] Z. Lv, J. Guo, A. K. Singh, and H. Lv, "Digital twins based VR simulation for accident prevention of intelligent vehicle," *IEEE Trans. Veh. Technol.*, vol. 71, no. 4, pp. 3414–3428, 2022.

[5] D. Song, R. Tharmarasa, T. Kirubarajan, and X. N. Fernando, "Multi-vehicle tracking with road maps and car-following models," *IEEE Trans. Intell. Transp. Syst.*, vol. 19, no. 5, pp. 1375–1386, 2017.

[6] Z. Tian, Y. Li, M. Cen, and H. Zhu, "Multi-vehicle tracking using an environment interaction potential force model," *IEEE Sens. J.*, vol. 20, no. 20, pp. 12 282–12 294, 2020.

[7] A. Ur-Rehman, S. M. Naqvi, L. Mihaylova, and J. A. Chambers, "Multi-target tracking and occlusion handling with learned variational Bayesian clusters and a social force model," *IEEE Trans. Signal Process.*, vol. 64, no. 5, pp. 1320–1335, 2015.

[8] P. Feng, W. Wang, S. Dlay, S. M. Naqvi, and J. Chambers, "Social force model-based MCMC-OCSVM particle PHD filter for multiple human tracking," *IEEE Trans. Multimedia*, vol. 19, no. 4, pp. 725–739, 2016.

[9] Y. Li and D. Sun, "Microscopic car-following model for the traffic flow: the state of the art," *J. Control Theory Appl.*, vol. 10, pp. 133–143, 2012.

[10] D. C. Gazis, R. Herman, and R. B. Potts, "Car-following theory of steady-state traffic flow," *Oper. Res.*, vol. 7, no. 4, pp. 499–505, 1959.

[11] P. G. Gipps, "A behavioural car-following model for computer simulation," *Transp. Res. B, Methodol*, vol. 15, no. 2, pp. 105–111, 1981.

[12] C. W. Reynolds, "Flocks, herds and schools: A distributed behavioral model," in *Proc. 14th Annu. Conf. Comput. Graph. Interact. Tech.*, 1987, pp. 25–34.

[13] D. Clark and S. Godsill, "Group target tracking with the gaussian mixture probability hypothesis density filter," in *Proc. Int. Conf. Intelli. Sensors, Sensor Netw. Inf.*, 2007, pp. 149–154.

[14] D. Song, R. Tharmarasa, G. Zhou, M. C. Florea, N. Duclos-Hindie, and T. Kirubarajan, "Multi-vehicle tracking using microscopic traffic models," *IEEE Trans. Intell. Transp. Syst.*, vol. 20, no. 1, pp. 149–161, 2018.

[15] Y. Cheng and T. Singh, "Efficient particle filtering for road-constrained target tracking," *IEEE Trans. Aerosp. Electron. Syst.*, vol. 43, no. 4, pp. 1454–1469, 2007.

[16] C. Hasberg, S. Hensel, and C. Stiller, "Simultaneous localization and mapping for path-constrained motion," *IEEE Trans. Intell. Transp. Syst.*, vol. 13, no. 2, pp. 541–552, 2011.

[17] M. Ulmke and W. Koch, "Road-map assisted ground moving target tracking," *IEEE Trans. Aerosp. Electron. Syst.*, vol. 42, no. 4, pp. 1264–1274, 2006.

[18] Y. Chen, V. P. Jilkov, and X. R. Li, "Multilane-road target tracking using radar and image sensors," *IEEE Trans. Aerosp. Electron. Syst.*, vol. 51, no. 1, pp. 65–80, 2015.

[19] K. Jo, M. Lee, J. Kim, and M. Sunwoo, "Tracking and behavior reasoning of moving vehicles based on roadway geometry constraints," *IEEE Trans. Intell. Transp. Syst.*, vol. 18, no. 2, pp. 460–476, 2016.

[20] K. Granström and M. Baum, "A tutorial on multiple extended object tracking," *Authorea Preprints*, 2023.

[21] J. W. Koch, "Bayesian approach to extended object and cluster tracking using random matrices," *IEEE Trans. Aerosp. Electron. Syst.*, vol. 44, no. 3, pp. 1042–1059, 2008.

[22] K. Granström, S. Reuter, D. Meissner, and A. Scheel, "A multiple model PHD approach to tracking of cars under an assumed rectangular shape," in *Proc. 17th Int. Conf. Inf. Fusion*. IEEE, 2014, pp. 1–8.

[23] M. Baum and U. D. Hanebeck, "Shape tracking of extended objects and group targets with star-convex RHMs," in *Proc. 14th Int. Conf. Inf. Fusion*, 2011, pp. 1–8.

[24] N. Wahlström and E. Özkan, "Extended target tracking using Gaussian processes," *IEEE Trans. Signal Process.*, vol. 63, no. 16, pp. 4165–4178, 2015.

[25] R. Mahler, "PHD filters for nonstandard targets, I: Extended targets," in *Proc. 12th Int. Conf. Inf. Fusion*, 2009, pp. 915–921.

[26] S. Blackman and R. Popoli, *Design and Analysis of Modern Tracking Systems*. Norwood, MA, USA: Artech House, 1999.

[27] R. Mahler, *Statistical Multisource-Multitarget Information Fusion*. Norwood, MA, USA: Artech House, 2007.

[28] B.-T. Vo and B.-N. Vo, "Labeled random finite sets and multi-object conjugate priors," *IEEE Trans. Signal Process.*, vol. 61, no. 13, pp. 3460–3475, 2013.

[29] S. Reuter, B.-T. Vo, B.-N. Vo, and K. Dietmayer, "The labeled multi-Bernoulli filter," *IEEE Trans. Signal Process.*, vol. 62, no. 12, pp. 3246–3260, 2014.

[30] Á. F. García-Fernández and L. Svensson, "Trajectory PHD and CPHD filters," *IEEE Trans. Signal Process.*, vol. 67, no. 22, pp. 5702–5714, 2019.

[31] B.-N. Vo and W.-K. Ma, "The Gaussian mixture probability hypothesis density filter," *IEEE Trans. Signal Process.*, vol. 54, no. 11, pp. 4091–4104, 2006.

[32] X. R. Li and V. P. Jilkov, "Survey of maneuvering target tracking. Part I. Dynamic models," *IEEE Trans. Aerosp. Electron. Syst.*, vol. 39, no. 4, pp. 1333–1364, 2003.

[33] G. Y. Kulikov and M. V. Kulikova, "Hyperbolic-SVD-based square-root unscented Kalman filters in continuous-discrete target tracking scenarios," *IEEE Trans. Autom. Control*, vol. 67, no. 1, pp. 366–373, 2021.

[34] X. Cao, C. Zhu, and W. Yi, "PHD filter based traffic target tracking framework with FMCW radar," in *Proc. 11th Int. Conf. Control, Autom. Inf. Sci.*, 2022, pp. 468–475.

[35] Y. Bar-Shalom, F. Daum, and J. Huang, "The probabilistic data association filter," *IEEE Control Syst. Mag.*, vol. 29, no. 6, pp. 82–100, 2009.

[36] D. Schuhmacher, B.-T. Vo, and B.-N. Vo, "A consistent metric for performance evaluation of multi-object filters," *IEEE Trans. Signal Process.*, vol. 56, no. 8, pp. 3447–3457, 2008.

[37] A. Rodriguez and A. Laio, "Clustering by fast search and find of density peaks," *Science*, vol. 344, no. 6191, pp. 1492–1496, 2014.

[38] X. Xue, S. Huang, J. Xie, J. Ma, and N. Li, "Resolvable cluster target tracking based on the DBSCAN clustering algorithm and labeled RFS," *IEEE Access*, vol. 9, pp. 43 364–43 377, 2021.